Effect of slope on smoke movement and temperature profile in underground utility tunnel

Ke Wang[1] · Ziping Lu[1] · Dong Wang[1] · Xiaodong Zhou[1] · Xiaoyu Ju[2] · Lizhong Yang[1]

Abstract

Underground utility tunnels with various municipal pipelines inside provide convenience for cities and contribute to their sustainable development, but also bring potential fire risks. Previously, the relevant studies have predominately focused on horizontal section, while ignoring the influence of slope at the intersection of utility tunnels. In the present study, the smoke movement and temperature distribution were investigated in utility tunnel fires with five slopes and six heat release rates by numerical simulation. Four different sizes of pool fire experiments were also conducted in a full-scale utility tunnel. The results indicated that: (1) Smoke movement can be divided into five stages, including free rise, diffusion under inclined ceiling, diffusion under horizontal ceiling, flow back, and steady circulation. (2) Temperature upstream is larger than that downstream of the fire source, which is asymmetrically distributed and shows different characteristics with the change in slope. (3) Downstream ceiling temperature decreases gradually with increasing distance from the fire source. An empirical formula is proposed to predict the downstream maximum ceiling temperature rise considering the slope and dimensionless heat release rate. Good agreement was obtained between predicted and experimental values.

Keywords Utility tunnel fire · Slope · Smoke movement · Maximum ceiling temperature

Abbreviations

a	Coefficient in Eq. (15)
A_f	Combustion area (m^2)
b	Coefficient in Eq. (15)
c_p	Air heat capacity (kJ kg^{-1} K^{-1})
D	Diameter of the equivalent circle (m)
D_i	Diffusion coefficient of the ith ingredient
D^*	Feature diameter of fire source (m)
f	Volume force vector
F_r	Froude number
g	Gravitational acceleration (m s^{-2})
H_d	Distance from fire source to the utility tunnel ceiling (m)
h	Height of the inclined section (m)
$h\prime$	Specific enthalpy, kJ kg^{-1}
k	Empirically calculated to be 1.1 (m^{-1})
K	Coefficient in Eq. (9)
$\dot{m}''$	Combustion rate (kg m^{-2} s^{-1})
$\dot{m}''_\infty$	Empirical combustion rate (kg m^{-2} s^{-1})
R	Correlation coefficient
p	Pressure (Pa)
q	Thermal radiation flux (kW m^{-2})
Q	Heat release rate of fire source (Kw)
$Q^\star$	Dimensionless fire heat release rate
t	Time (s)
T_a	Ambient temperature (K)
ΔH_c	Complete heat of combustion (MJ kg^{-1})
ΔT_{max}	Maximum excess ceiling temperature (K)
u	Longitudinal ventilation velocity (m s^{-1})
$\boldsymbol{u}$	Velocity vector
x	Horizontal distance from the fire source (m)
Y_i	Mass fraction of the ith ingredient

Greek symbols

α	Slope of the inclined section (%)
β	Coefficient in Eq. (4)
γ	Coefficient in Eq. (12)
ε	Coefficient in Eq. (4)
θ	Slope of the tunnel (%)
δ	Grid size (m)

✉ Xiaoyu Ju
  xju@berkeley.edu

✉ Lizhong Yang
  yanglz@ustc.edu.cn

1 State Key Laboratory of Fire Science, University of Science and Technology of China, Hefei 230026, Anhui, China

2 Department of Mechanical Engineering, University of California, Berkeley, CA 94702-5800, USA

ρ	Density, kg m^{-3}
ρ_a	Air density (kg m^{-3})
τ	Viscous tension per unit area
ψ :	Coefficient in Eq (14)
χ	Combustion efficiency
Φ	Dissipation rate (kW m^{-3})

Introduction

If a city is regarded as a living body, urban underground utility tunnels are similar to arteries that transport electricity, water, gas, etc. It guarantees that the city operates normally and steadily, which is precisely why it is called the "lifeline" [1]. Urban underground utility tunnels not only improve the utilization of urban land resources but also facilitate the unified management and maintenance of multiple pipelines by municipal departments, which is an important infrastructure in the process of urban modernization and is conducive to the sustainable development of cities [2–4]. Many countries are now increasing in the construction of utility tunnels, especially in China, Japan and some countries in Europe [5]. Nevertheless, while it provides convenience, the centralized placement of these pipelines also poses additional potential risks [6, 7].

Cables in utility tunnels give off heat and age over time, making cable fires one of the most common hazards. For example, in 2017, the U.S. Atlanta International Airport lost power due to underground cable fires, causing 1,173 flights to be canceled and thousands of passengers to be stuck. In 2018, a utility tunnel cable fire in Xi'an, China, caused an explosion at a nearby transformer station, breaking off the power supply to the immediate area for approximately 44 h [8].

In recent years, many scholars have studied fire in underground utility tunnels. Liang studied the smoke spreading process and temperature distribution of T-shaped horizontal underground utility tunnel fires and found inconsistencies in smoke layer thickness and temperature in different regions [9]. An modeled an L-shaped horizontal underground utility tunnel by numerical simulation and studied the CO diffusion of cable fires with different cable inclination angles,

fire source power and ventilation [10]. Mi studied the temperature and visibility of a 200-m-long horizontal underground utility tunnel fire and obtained the best combination of ventilation, fire-proof doors and sprinkler systems [11]. Pan experimentally studied the effect of curved sidewalls on the fire shape and maximum temperature beneath the ceiling centerline in horizontal underground utility tunnels [12]. Ye obtained the longitudinal decay law of the maximum temperature of the ceiling jet driven by a strong plume in a horizontal underground utility tunnel through full-scale experiments and established a two-dimensional temperature prediction method [1, 13]. Gao studied the thermal flow propagation and ceiling temperature distribution in a horizontal underground utility tunnel and obtained the maximum ceiling temperature predictive equations for near-field and far-field energy sources [14]. Through fire experiments of a single-layer cable in a horizontal utility tunnel, Huang obtained a model for predicting the maximum excess ceiling temperature [15]. These studies provide valuable references for the design of fire protection in underground utility tunnels.

Most previous studies have focused on horizontal utility tunnel fires but neglected the case of inclined utility tunnels. Utility tunnels are generally laid straight underground along roads; however, at the intersection of two roads, as utility tunnels cannot intersect directly, a sunk structure is formed, including the upper horizontal section, inclined section, and lower horizontal section, as shown in Fig. 1. As the number of road and utility tunnel constructions increases, this type of structure is becoming increasingly common. However, fire progressions and temperature profiles are unknown in the narrow and enclosed area, making firefighting and rescue extremely difficult. The study of smoke movement and temperature field distribution of fires in this region can help to predict the trend of fire development and can provide a valuable reference for fire rescue. Figure 2 shows the interior of the inclined section of a newly constructed cable cabin in a utility tunnel. In this study, FDS is used to simulate utility tunnel fires to investigate the effects of slope on smoke movement and temperature profile. Four different sizes of pool fire experiments were also conducted. The results of the

Fig. 1 Underground utility tunnels connection at crossroads
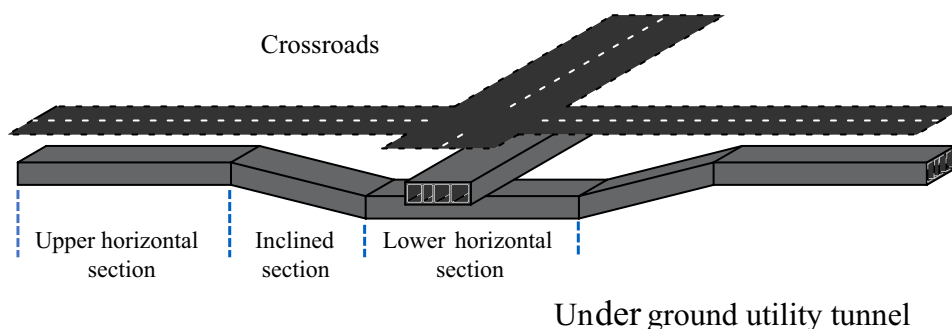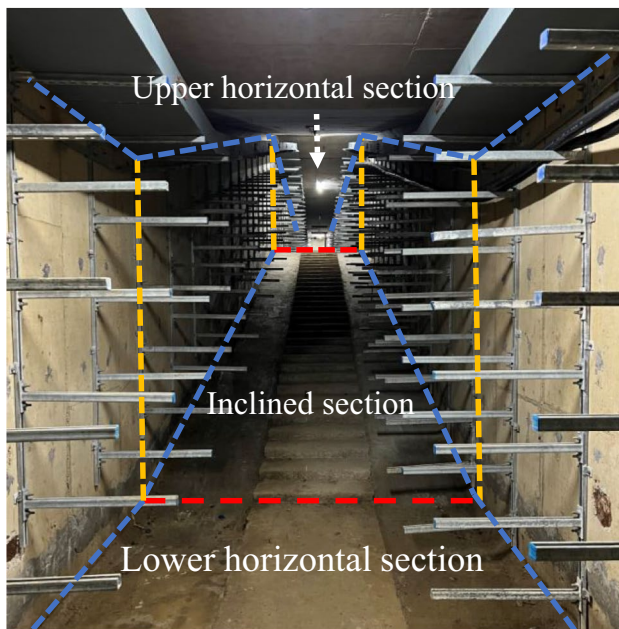
Fig. 2 Inclined section of the cable cabin in the utility tunnel

study can provide guidance for utility tunnel fire protection design, such as angle design of inclined sections and fire detector placement.

Numerical simulation

FDS introduction

FDS (fire dynamics simulator) was developed by the National Institute of Standards and Technology (NIST) to calculate the flow of fluids driven by fire. The version used in this study is FDS 6.7.6. FDS solves the Navier–Stokes equations for low-velocity, thermally driven flow with a numerical method, focusing on the transportation of smoke and heat generated by fire. The equation accurately reflects the distribution of velocity, temperature, pressure and other parameters in a real fire scenario by characterizing the low-velocity flow under buoyancy drive. FDS includes two numerical simulation models, direct numerical simulation (DNS) and large-eddy simulation (LES) [16]. For large structures such as utility tunnels and traffic tunnels, large-eddy simulation (LES) based on the Smagorinsky [17] model can guarantee both computational accuracy and resource savings and has been widely used in utility tunnel and traffic tunnel fire studies [14, 16, 18–20]. The basic control equations are as follows:

(1) Energy conservation equation:

$$\frac{\partial}{\partial t}\left(\rho h'\right) + \nabla \cdot \rho h' \boldsymbol{u} = \frac{Dp}{Dt} + \dot{q}''' - \nabla \cdot q + \Phi \tag{1}$$

where ρ is the density, kg m^{-3}; $h\prime$ is the specific enthalpy, kJ kg^{-1}; ∇ is the Hamiltonian operator; $\boldsymbol{u}$ is the velocity vector; p is the pressure, Pa; t is the time, s; $\dot{q}'''$ is the heat release rate, kW m^{-3}; q is the thermal radiation flux, kW m^{-2}; and Φ denotes the dissipation rate, kW m^{-3}.

(2) Mass conservation equation

$$\frac{\partial \rho}{\partial t} + \nabla \cdot \rho \boldsymbol{u} = 0 \tag{2}$$

(3) Momentum conservation equation

$$\frac{\partial}{\partial t}(\rho \boldsymbol{u}) + \nabla \cdot \rho \boldsymbol{u}\boldsymbol{u} + \nabla p = \rho g + \boldsymbol{f} + \nabla \cdot \boldsymbol{\tau} \tag{3}$$

where g is the acceleration of gravity; $\boldsymbol{f}$ is the volume force vector; and $\boldsymbol{\tau}$ is the viscous tension per unit area.

(4) Component transport equation

$$\frac{\partial}{\partial t}\left(\rho Y_i\right) + \nabla \cdot \rho Y_i \boldsymbol{u} = \nabla \cdot \rho D_i \nabla Y_i + \dot{m}_i''' \tag{4}$$

where Y_i is the mass fraction of the ith ingredient; D_i is the diffusion coefficient of the ith ingredient; and $\dot{m}_i'''$ is the mass production rate of the ith ingredient.

Utility tunnel modeling setup

In the actual utility tunnel design, the entire sunken area is taken as a section of fire partition with fire doors at both ends, and the distance is generally no more than 200 m. Due to the approximately symmetrical structure of the sunken section of the utility tunnel, half of the area is selected to study the development of fire in this paper. The horizontal length of the full-size utility tunnel model is 100 m in total, including 38 m for the upper horizontal section, 24 m for the inclined section and 38 m for the lower horizontal section. Its cross-sectional width and height are 2.8 m and 3.2 m, respectively. According to the actual situation, the left end of the upper horizontal section is set to be closed due to the presence of a fire door, and the right end of the lower horizontal section is set to be open due to the connection with the upper level utility tunnel to ensure the flow of air. This setup has been effectively applied in previous numerical simulations and full-scale experimental studies of utility tunnel fires [13, 14]. Compared to a traffic tunnel, the inclined section of the utility tunnel is steeper. The geometry and measurement points of the utility tunnel model are shown in Fig. 3, where h and α are the height and slope of the inclined section, respectively. By changing h to 0 m, 3 m, 6 m, 8 m and 12 m, the slope α is made to be 0, 1/8, 1/4, 1/3, and 1/2,

Fig. 3 Geometry and measurement points of the utility tunnel model

(a) Side view

(b) Top view

(c) Meshing diagram
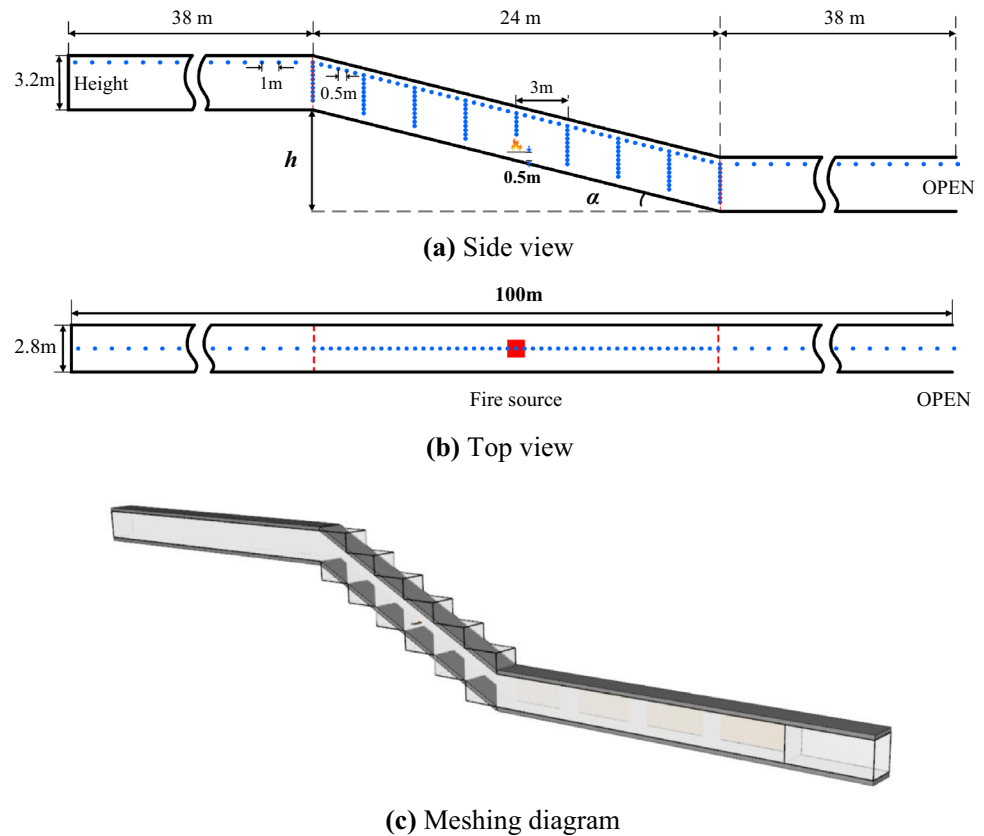
respectively. The lower horizontal end boundary condition is set to "OPEN," and the interior of the utility tunnel is set to natural ventilation with no initial ventilation velocity. All wall materials are set to "CONCRETE," and their thermal properties mainly include conductivity, density and specific heat, which are set to 1.8 W m^{-1} K^{-1}, 2280 kg m^{-3} and 1.04 kJ^{-1} kg^{-1} K^{-1}), respectively. The ambient temperature is 20 °C, and the ambient pressure is 101.325 kPa. In this paper, n-heptane is used as the fire source, and the size of the fire source is simplified to 1 m × 1 m because the cables are generally closely arranged to approximate a rectangle. The position is set at a height of 0.5 m from the ground in the middle of the inclined section to simulate the lowermost cable fire. The average heat release rate of real cable is approximately 265 kW m^{-2} [10]. The burning area of each cable layer is approximately 4 m^2, and the calculated fire heat release rate is set to 1 MW, 2 MW and 3 MW when the number of cable layers is 1 to 3.

Grid sensitivity analysis

In FDS, the grid size has a decisive influence on the simulation time and the accuracy of the simulation results. McGrattan [21] proposed that reliable results can be obtained when the ratio of the grid size δ to the fire source feature diameter D^* is between 1/16 and 1/4. Using this setup, previous scholars obtained the desired validation results after comparison with experimental data [16, 20]. D^* is denoted as:

$$D^* = \left(\frac{Q}{\rho_a c_p T_a \sqrt{g}} \right)^{\frac{2}{5}} \tag{5}$$

The grid size suitable for the heat release rate of the fire source in this paper is between 0.08 and 0.26 m, as calculated by Eq. (5). A smaller grid would better reflect the details of the heat flow field, but the time would also increase dramatically [18]. To balance the calculation time and accuracy, five grid sizes of 0.25 m, 0.20 m, 0.16 m, 0.10 m, and 0.08 m, i.e., 4 ~ 12 grids per meter, are selected to estimate the sensitivity of the grid size. Figure 4 shows the vertical temperature distribution under the ceiling at 3 m from the fire source at a slope of 0. The larger grid overcalculates the temperature at the central location and underestimates the temperature near the ceiling. As the grid size decreases, the temperature profiles gradually tend to be uniform. When the grid size is less than 0.10 m, there is no significant improvement, but the time consumption increases. Considering the calculation efficiency, 0.1 m is finally chosen as the grid size.
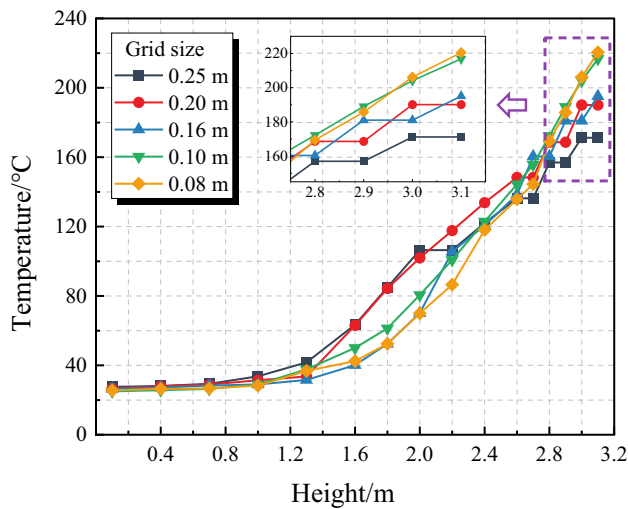
Fig. 4 Vertical temperature distribution under the ceiling at 3 m from the fire source

Experimental

The experiment was conducted in a newly constructed underground utility tunnel with a fire-proof door at one end, and the schematic sketch of the experiment is shown in Fig. 5. Due to the limitations of the experimental sites, we were unable to conduct experiments at site of the same length as the numerical model. The total length of the inclined section is 10 m, and the horizontal distance from the fire door is 3 m. The slope of the inclined section is 0.25, and the width and height of its cross section are 2.8 m and 3.2 m, respectively. A pool fire was used as the fire source, fueled

by n-heptane and positioned in the middle of the inclined section. The heat release rate of the fire is varied by changing the side length of the square oil pan to 20 cm, 25 cm, 30 cm and 35 cm. The fire heat release rate is calculated by the following equation:

$$\dot{Q} = A_f \dot{m}'' \chi \Delta H_c \tag{6}$$

where $\dot{Q}$ is the heat release rate, A_f is the fuel combustion area, $\dot{m}''$ is the combustion rate, χ is the combustion efficiency taken as 0.7[22], and ΔH_c is the heat of complete combustion value of 44.6 MJ kg^{-1}[22]. For n-heptane, $\dot{m}''$ can be calculated by the following equation:

$$\dot{m}'' = \dot{m}''_\infty \bullet \left(1 - e^{-kD}\right) \tag{7}$$

$\dot{m}''_\infty$ is empirically calculated to be 0.101 (kg m^{-2}s), k is empirically calculated to be 1.1 (m^{-1}) and D is the diameter of the equivalent circle. The calculated heat release rates for each pan are shown in Table 1. In addition, thermocouple trees were arranged at 1-m intervals upstream and downstream of the fire source in the inclined section for a total of 10 thermocouple trees. Each thermocouple tree was arranged with K-type thermocouples from top to bottom to measure the temperature.

Results and discussion

Smoke movement and temperature distribution

Due to the low density of the hot smoke from the utility fire, thermal pressure is formed between it and the air. Driven
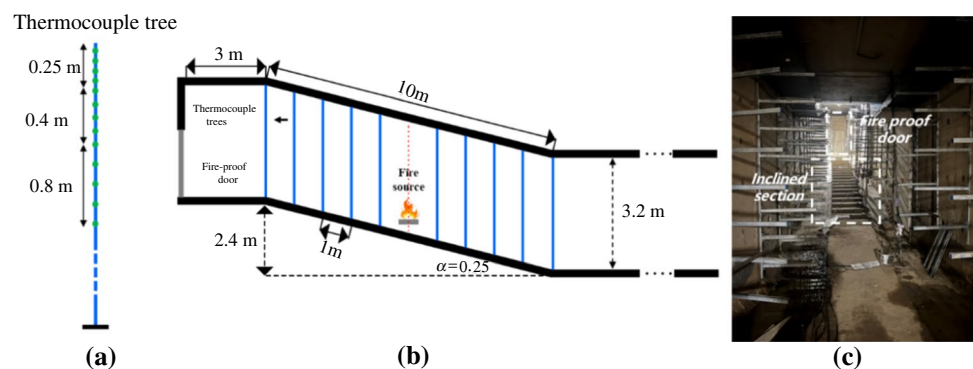
Fig. 5 Schematic sketch of the experiment

Table 1 Calculated HRRs for oil pans of different sizes

Fuel	ΔH_c/MJ kg^{-1}	Pan Size/cm×cm	A_f/m^2	D/m	HRRs/kW
n-Heptane	44.6	20×20	0.0400	0.2257	22.73
		25×25	0.0625	0.2821	52.58
		30×30	0.0900	0.3385	88.23
		35×35	0.1225	0.3949	136.11

by the buoyancy generated by the thermal pressure, the hot smoke first rises freely. Then, due to the obstruction of the wall, the smoke will spread longitudinally along the utility tunnel ceiling [23]. In the utility tunnel sunk area studied in this paper, the stack effect occurs owing to the height difference between the two ends of the inclined section. The velocity of the airflow induced by the stack effect increases as the slope increases and changes the position of the flame hitting the ceiling [24].

As shown in Fig. 6, the filling of the smoke in the utility tunnel can be divided into five stages when the slope of the inclined section is 1/4, for example. Other slope cases have the same characteristics of smoke movement and are not repeatedly expressed. I. The smoke is driven by thermal buoyancy and rises freely under the ceiling. II. When the plume hits the wall above, it begins to spread longitudinally along the sloping ceiling. The diffusion of the smoke to the two ends of the utility tunnel is not symmetrical under the influence of the stack effect. The diffusion of smoke to

Fig. 6 Stages of smoke movement in the utility tunnel by simulation

the upper horizontal section is faster than that to the lower horizontal section. III. When the smoke reaches the upper horizontal section, the smoke moves toward the closed end. Since there is no air exchange with the outside at the closed end, the air is pressed by the hot smoke to create a flow in the opposite direction below the smoke layer. The diffusion of airflow in the lower layer produces an entrainment effect on the smoke in the upper layer, thickening the smoke layer. IV, when the smoke moves to the closed end, due to the fire door blocking, the smoke begins to flow back and gradually fills the entire upper horizontal section. V. The smoke fills the entire upper horizontal section and the area above the inclined section, creating a steady diffusion cycle. Eventually, the smoke diffuses from the lower horizontal section to the outside. The upper part is the hot smoke layer flowing outward, and the lower part is the cold air layer flowing inward, forming a stable thermal stratification so the smoke layer is approximately horizontal. Figure 7 shows the filling process of the smoke during the experiment, which is in good agreement with the simulation. Figure 8 shows the distribution of the flow field superimposed on the velocity field for slopes of 0 and 1/4. The presence of the inclined section changes the smoke movement, which is significantly different compared to the horizontal utility tunnel. In the inclined section, the hot smoke near the ceiling moves faster upstream of the fire source and slower downstream of the fire source due to the stack effect. The air flow velocity near the ground also increases, causing hot smoke to flow faster to the ground, resulting in higher temperatures near the ground than in horizontal tunnels.

To study the effect of slope change on temperature distribution in the inclined section, Fig. 9 shows the distribution of temperature in the steady diffusion stage of smoke when the slope is 0, 1/8, 1/4, 1/3 and 1/2. When the slope is 0, the smoke flows back due to the closed left port, so that more smoke collects at the left end of the fire source and its high-temperature area is larger compared to the right end of the fire source. As the slope of the inclined section increases, under the influence of the stack effect, the smoke mainly gathers in the upper horizontal section.
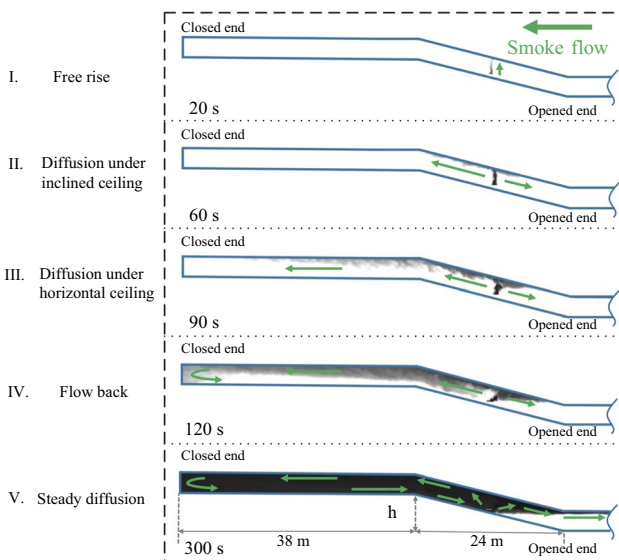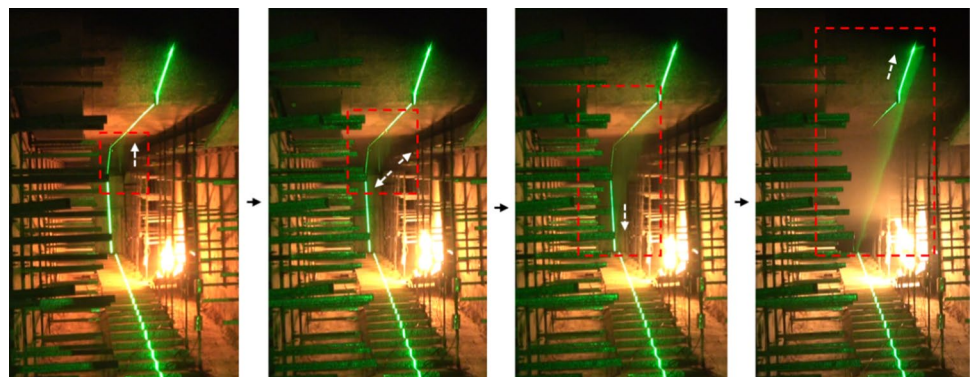
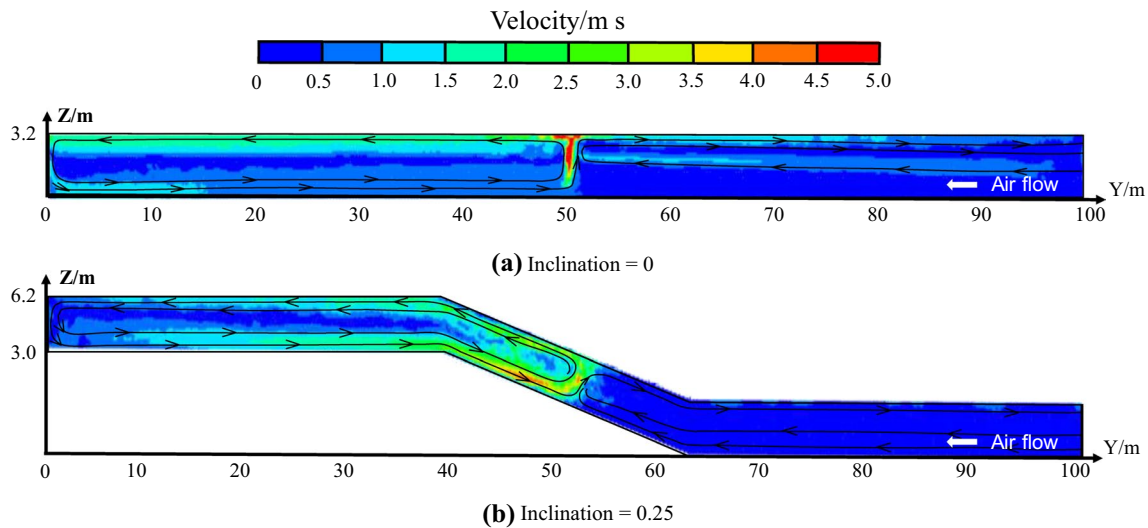**Fig. 7** Smoke filling progress in the experiment

Fig. 8 Distribution of the flow field superimposed with the velocity field

This makes the overall temperature of the upper horizontal section higher than that of the lower horizontal section, and the high-temperature area of the lower horizontal section is mainly concentrated under the ceiling.

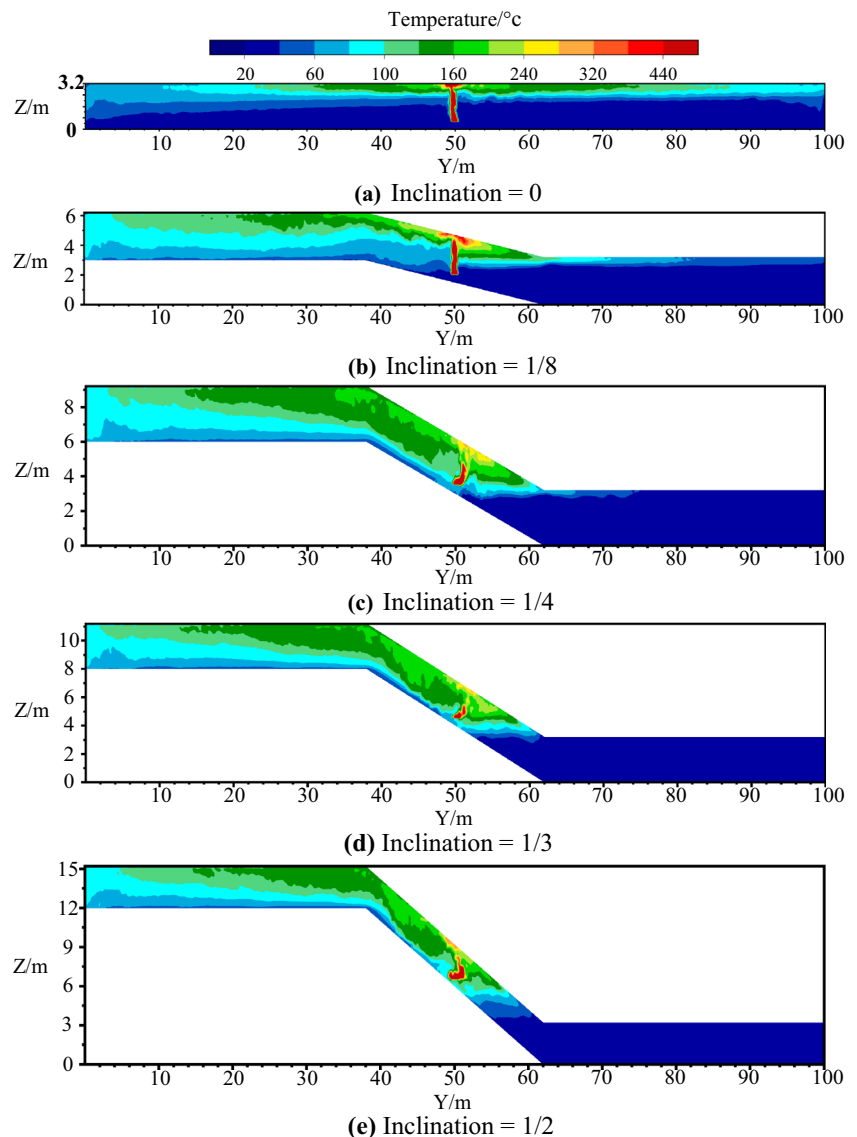## Vertical temperature distribution

As described in earlier, the stack effect caused by the presence of the inclined section has a large impact on the temperature distribution in the utility tunnel. To study the vertical temperature distribution in the inclined section, thermocouple trees were set up at 3-m, 6-m and 9-m upstream and downstream of the fire source. Figure 10 and Fig. 11 show the variation of vertical temperature with time at different locations upstream and downstream from the fire source, respectively. For the fire source, the heat release rate is 1 MW, and the slope of the inclined section is 1/4. The vertical temperature of the inclined section tends to increase gradually with the development of fire, and when the steady diffusion stage of the smoke is reached, the temperature at each location basically ceases to change. It also shows that the simulation time selected meets the demand. Upstream of the fire source, the vertical temperatures all increase. As the height decreases, the temperature falls gently. Downstream of the fire source, there is an increase in temperature near the ceiling, and the temperature is almost constant near the ground. The vertical temperature drop is more dramatic than the upstream temperature drop. This is because the upstream smoke fills the entire upper horizontal section and flows near both the ceiling and the ground, while the downstream smoke flows only near the ceiling. Notably, unlike conventional road tunnels, the upstream circulating flow causes the

flame to tilt in the downstream direction. The hot smoke moves along the ceiling to the upper horizontal section, and because it is blocked by the fire door, the smoke flows toward the ground and flows along the ground to the fire source. As shown in Fig. 8b, this part of the smoke is mainly entrained to the ceiling via the fire and moves downstream, thus driving the fuel vapor downstream and causing the flame to tilt in the downstream direction. The temperature close to the flame is higher due to the greater thermal radiation received. Figures 10a and 11a show that the temperature near the ceiling at 3-m upstream of the fire source is less than that at 3-m downstream of the fire source, also indicating that the flame is tilted downstream. In addition, the vertical temperature distribution has a "convex" shape, which is consistent with Oka's [25, 26] study and verifies the reliability of the FDS data.

The vertical temperatures upstream and downstream of the fire in the experiment are shown in Fig. 12. The temperature upstream at the same distance from the fire source is higher than that downstream, while the temperature near the ground downstream is not significantly higher, which verifies the accuracy of smoke movement and temperature data in FDS.

To study the effect of slope, Fig. 13 shows the vertical temperature distribution at different locations upstream and downstream during the steady development stage of the fire in the inclined section. The distances of 9 m and 12 m from the fire source were chosen to exclude the insignificant change in vertical temperature distribution with slope due to the proximity to the fire source. From Fig. 13a and b, it can be found that the upstream temperature of the inclined section tends to increase gradually when the slope increases, while the vertical temperature does not change

Fig. 9 Temperature distribution in inclined sections with different slopes

(a) Inclination = 0

(b) Inclination = 1/8

(c) Inclination = 1/4

(d) Inclination = 1/3

(e) Inclination = 1/2

much when the slope reaches 1/4, 1/3 and 1/2. Figure 13c and d shows that as the slope increases, the movement of the smoke downstream becomes increasingly difficult under the influence of the stack effect, and the thickness of the smoke layer downstream gradually decreases, leading to a vertical temperature decrease.

Downstream longitudinal temperature decay

Figure 14 shows the distribution of maximum temperature at 0.1 m from the ceiling with increasing slope. Similar to the vertical temperature distribution law, with the increase in the slope of the inclined section, the longitudinal temperature distribution upstream of the fire source is almost unchanged after the slope increases to 1/4, and the maximum ceiling temperature rise downstream of the fire source shows an obviously different decay law with the increase in the horizontal

distance. Traffic tunnels and utility tunnels have similar geometrical characteristics in terms of building structure, and previous research and analysis of the maximum excess ceiling temperature in traffic tunnels is of some guidance.

Kurioka [27] established a maximum excess ceiling temperature model by conducting multiple sets of experiments within a small-sized horizontal tunnel of 1:10 as follows:

$$\frac{\Delta T_{\max}}{T_a} = \beta \left(\frac{Q^{\star 2/3}}{F_r^{1/3}} \right)^{\varepsilon}$$
$$Q^{*2/3}/F_r^{1/3} < 1.35, \beta = 1.77, \varepsilon = 1.2$$
$$Q^{*2/3}/F_r^{1/3} \geq 1.35, \beta = 2.54, \varepsilon = 0$$

$$(8)$$

where T_a is the ambient temperature, the coefficients β and ε are constants. Q^* is the dimensionless heat release rate and F_r represents the Froude number depending on Eq. (9) and Eq. (10), respectively.

(a) Upstream 3 m

(b) Upstream 6 m

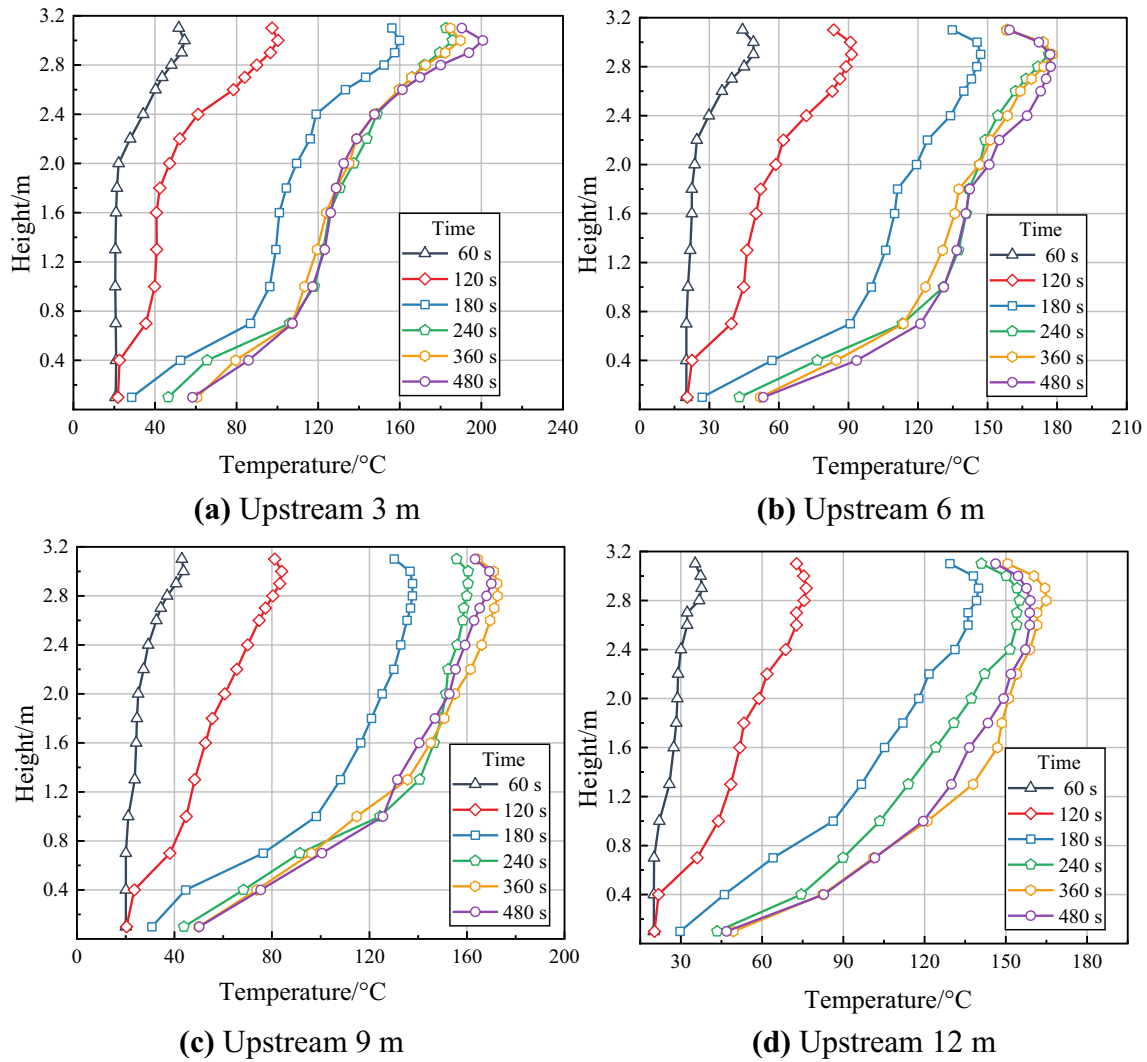**(c)** Upstream 9 m

(d) Upstream 12 m

Fig. 10 Vertical temperature distribution upstream (HRR = 1 MW, slope = 1/4)

$$Q^* = \frac{Q}{\rho_a c_p T_a g^{1/2} H_d^{5/2}} \tag{9}$$

$$F_r = \frac{u^2}{gH_d} \tag{10}$$

where ρ_a is the ambient air density, c_p is the air heat capacity, g is the gravitational acceleration, H_d is the distance from the fire source to the utility tunnel ceiling and u is the longitudinal ventilation velocity. However, in the natural ventilation case, $F_r = u^2/gH_d$ tends to 0, and the calculation of Q^* by Eq. (9) tends to infinity and is obviously not applicable. Based on plume theory, Li [28] obtained the maximum excess ceiling temperature prediction equation for axisymmetric pool fires in naturally ventilated traffic tunnels. ΔT_{max} is expressed as:

$$\Delta T_{max} = 17.5 \frac{Q^{2/3}}{H_d^{5/3}} \tag{11}$$

Both Kurioka's and Li's models do not consider the effect of the ceiling slope. Hu[29] obtained the maximum excess ceiling temperature model under natural ventilation and the longitudinal temperature decay equation by conducting gas fire experiments in model tunnels with 0%, 3% and 5% slopes, taking into account the tunnel slope factor, as shown in Eqs. (12) and (13):

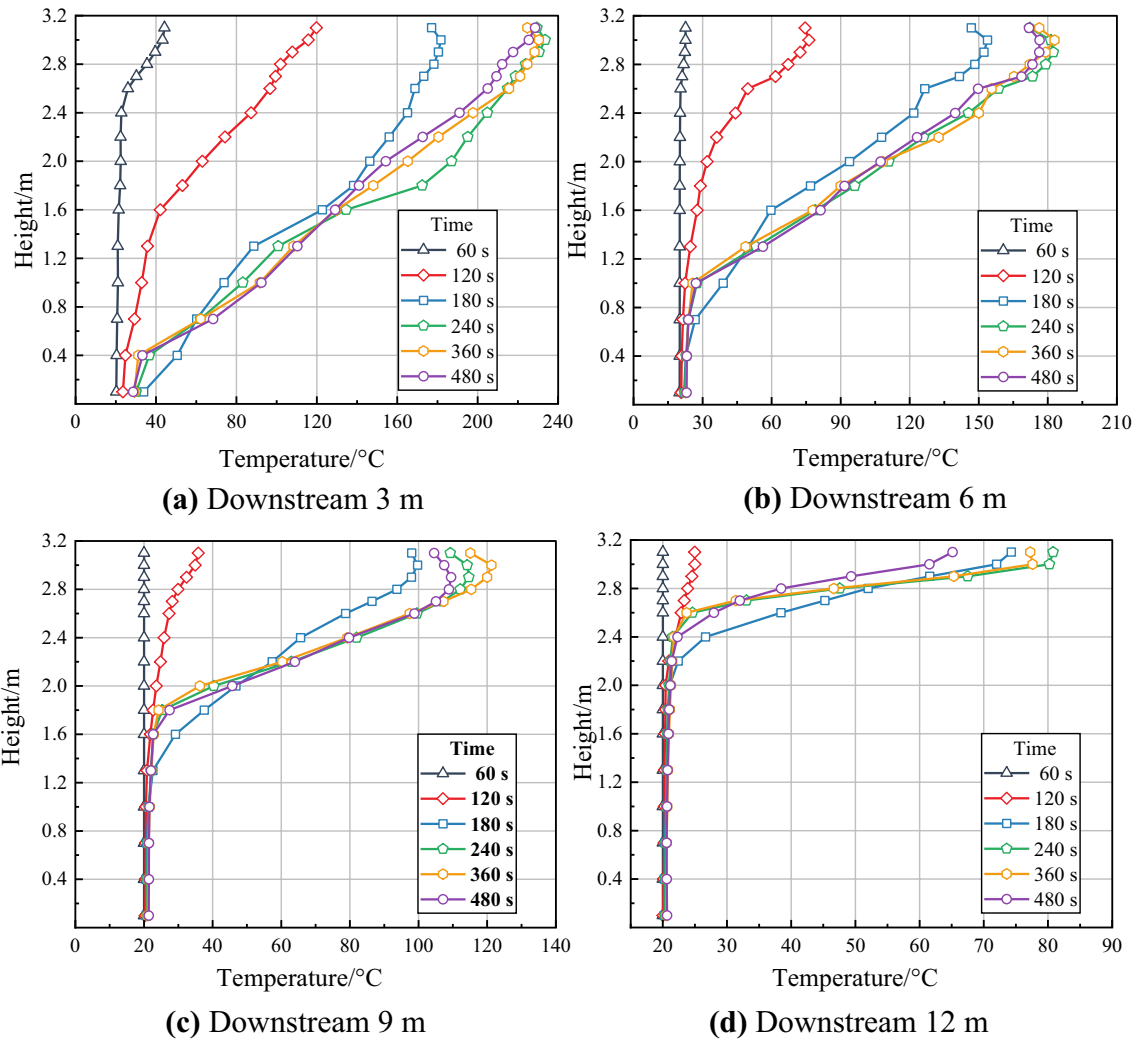$$\Delta T_{max} = (1 - 0.061\theta)\frac{17.5Q^{2/3}}{H_d^{5/3}} \tag{12}$$

(a) Downstream 3 m   **(b)** Downstream 6 m

(c) Downstream 9 m   **(d)** Downstream 12 m

Fig. 11 Vertical temperature distribution downstream (HRR = 1 MW, slope = 1/4)

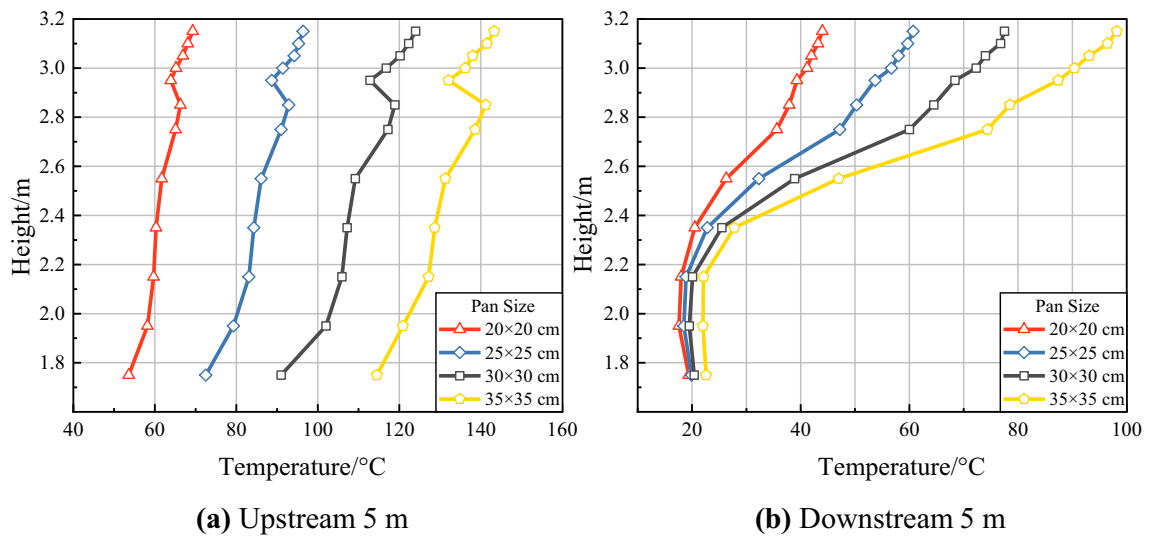**(a)** Upstream 5 m   **(b)** Downstream 5 m

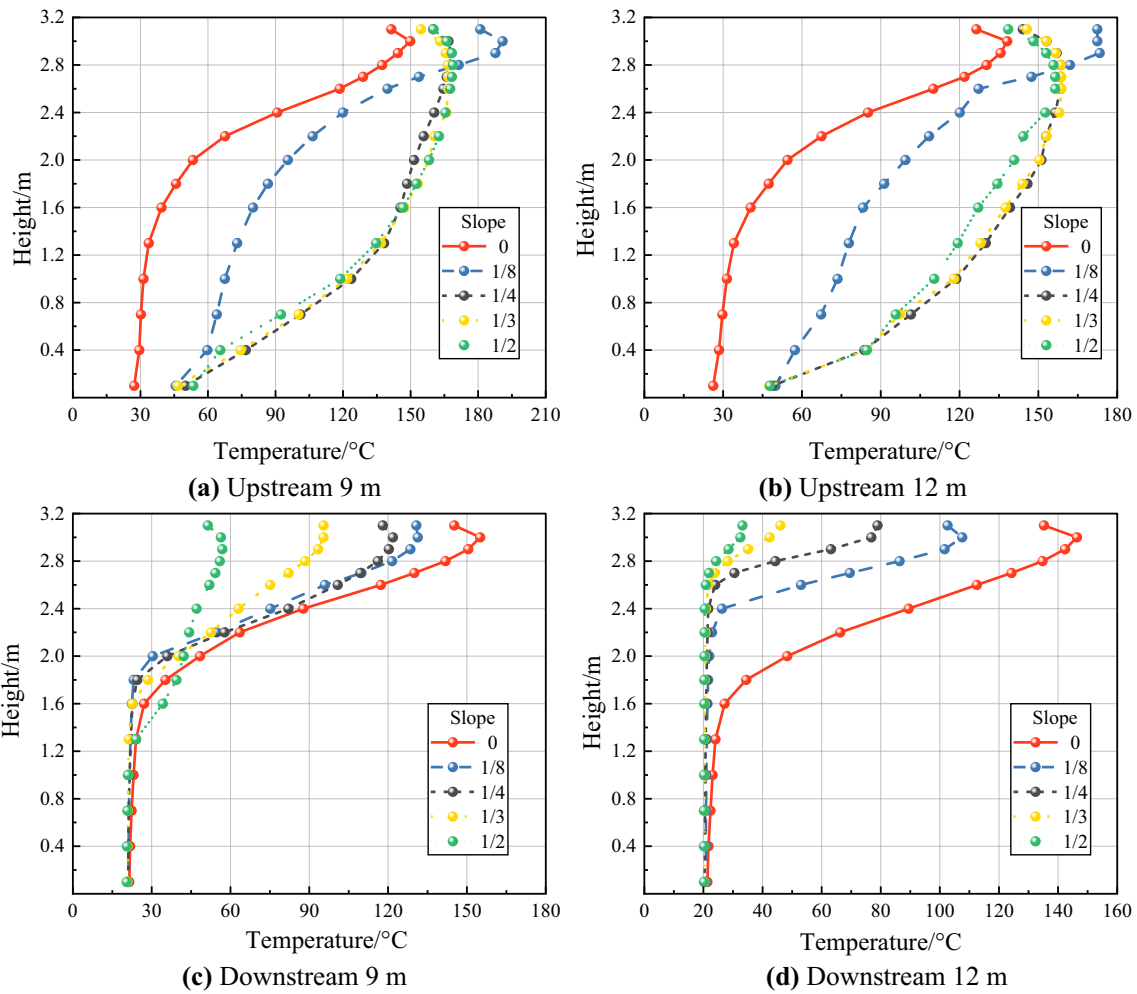**Fig. 12** Vertical temperature distribution upstream and downstream in the experiment

Fig. 13 Variation of the vertical temperature distribution with slope (HRR = 1 MW)

$$\frac{\Delta T_{max,x}}{\Delta T_{max}} = e^{-(1+0.09\theta)Kx} \tag{13}$$

where θ is the slope of the tunnel (%) and x is the horizontal distance of the measurement point from the fire source. Ji [16] conducted simulations of tunnel fires at more inclination angles by FDS and obtained another model of maximum excess temperature under an inclined ceiling:

$$\frac{\Delta T_{max,x}}{T_a} = Q^{*0.56}\left(2.37 + 0.89e^{16.10\theta}\right)e^{\left(-0.05-166.38\theta^{2.31}\right)\left(\frac{x}{H_d}\right)} \tag{14}$$

In this study, the dimensionless maximum excess ceiling temperature at steady diffusion is expressed as:

$$\Delta T_{max,d} = \frac{T_{max,x} - T_a}{T_a} = \frac{\Delta T_{max,x}}{T_a} \tag{15}$$

Based on the previous model, an exponential function can be used for fitting. To exclude the instability of the longitudinal temperature decay caused by flame tilt, only the case of
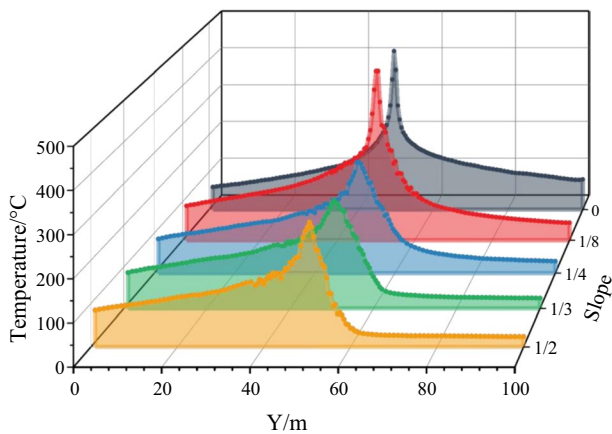
Fig. 14 Longitudinal maximum ceiling temperature distribution (HRR = 1 MW)

the far field of the fire source ($x/H_d > 1$) is considered [14]. The downstream longitudinal temperature decay of the fire source can be considered to be in accordance with Eq. (16).

$$\frac{\Delta T_{\mathrm{max,x}}}{T_a} = \psi e^{\gamma\left(\frac{x}{H_d}\right)} \tag{16}$$

where ψ and γ are the fitting coefficients, and Fig. 15 shows that the coefficients are related to the fire HRR and the slope.

Table 2 records the fitted ψ and γ for different fire source heat release rates and slopes, as well as the correlation coefficient R. ψ is positive and increases gradually with increasing slope. γ is negative and decreases with increasing slope. The correlation coefficients, R, were all greater than 0.95, indicating the accuracy of the fitted curves.

Figures 15 and 16 show the variation of the coefficients ψ and γ with slope. At the same slope, ψ increases with increasing fire source heat release rate, while γ is almost
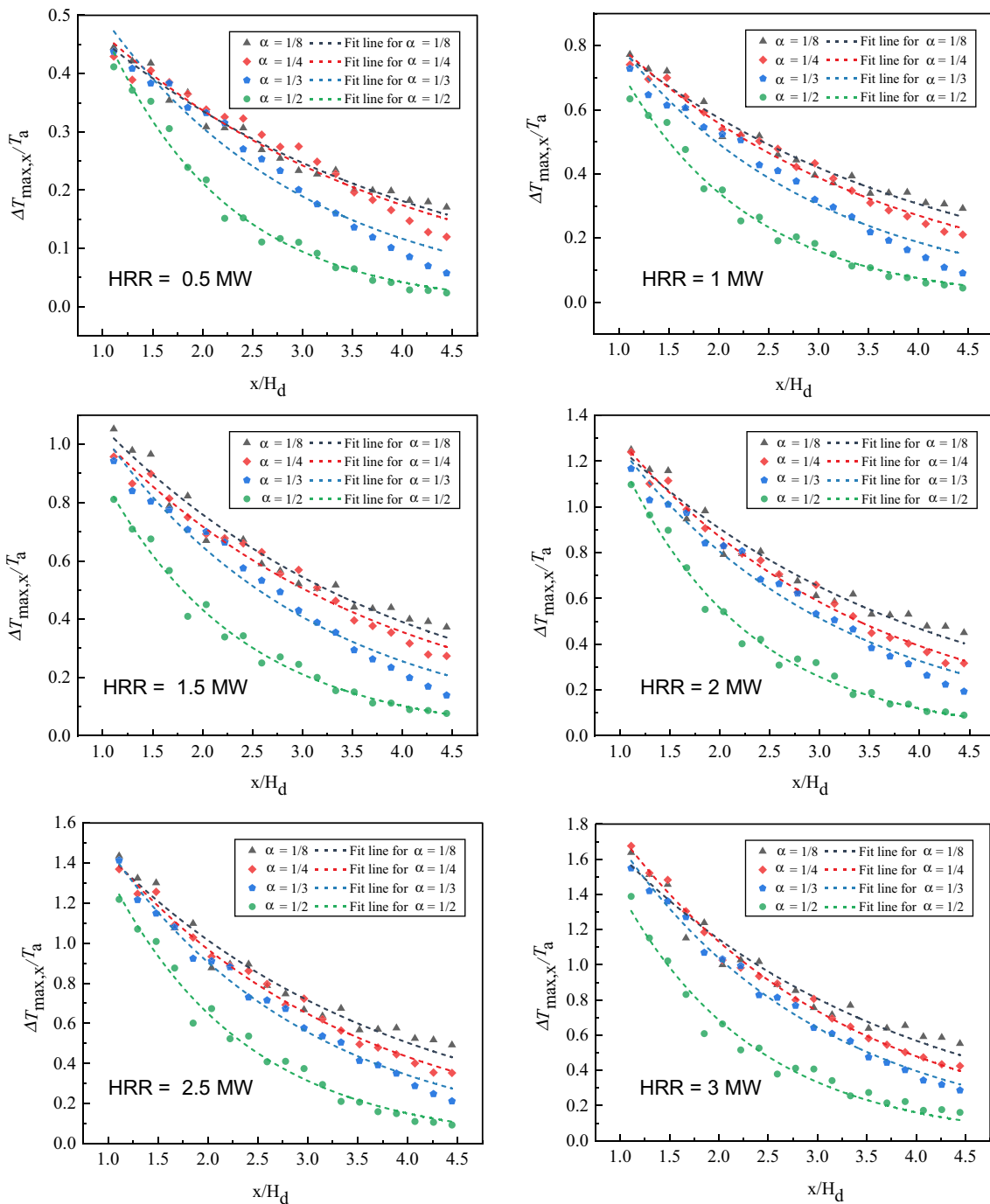
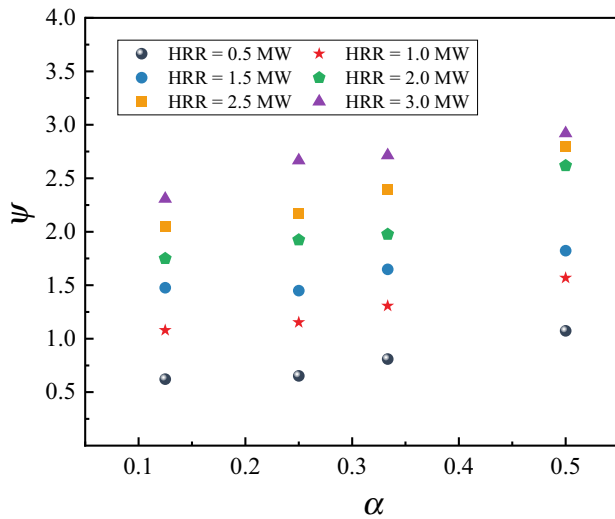**Fig. 15** Dimensionless maximum excess ceiling temperature

Fig. 16 Variation of coefficient ψ

Fig. 17 Variation of coefficient γ with slope α

constant. It is shown that the coefficient ψ is related to the fire HRR Q and the slope α, while the coefficient γ is only related to the slope α.

$$\psi = f(Q, \alpha) \tag{17}$$

$$\gamma = f(\alpha) \tag{18}$$
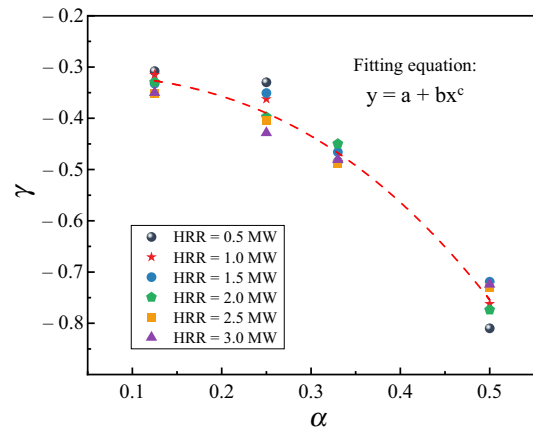
Since the maximum excess temperature is a function of the fire HRR, Fig. 17 shows the variation of ψ with the dimensionless HRR Q^* and is fitted using Eq. (19):

$$\psi = aQ^{*b} \tag{19}$$

From the fitting results, the power exponents are found to be approximately the same. The results of previous studies are mostly related to the constant power of the dimensionless heat release rate Q^*, so the average value of b, 0.711, is used as the power exponent, as in Eq. (20).

Table 2 Fitted coefficients ψ and γ

HRR = 0.5 MW				HRR = 1 MW			
Slope	ψ	γ	R	Slope	ψ	γ	R
1/8	0.622	−0.308	0.978	1/8	1.079	−0.315	0.973
1/4	0.652	−0.330	0.956	1/4	1.152	−0.363	0.986
1/3	0.810	−0.484	0.962	1/3	1.306	−0.486	0.965
1/2	1.074	−0.810	0.986	1/2	1.568	−0.762	0.985
HRR = 1.5 MW				HRR = 2 MW			
Slope	ψ	γ	R	Slope	ψ	γ	R
1/8	1.476	−0.332	0.969	1/8	1.749	−0.330	0.964
1/4	1.449	−0.351	0.978	1/4	1.923	−0.398	0.990
1/3	1.649	−0.466	0.970	1/3	1.976	−0.450	0.976
1/2	1.823	−0.720	0.986	1/2	2.618	−0.774	0.987
HRR = 2.5 MW				HRR = 3 MW			
Slope	ψ	γ	R	Slope	ψ	γ	R
1/8	2.046	−0.351	0.966	1/8	2.307	−0.350	0.960
1/4	2.172	−0.403	0.991	1/4	2.666	−0.429	0.993
1/3	2.398	−0.487	0.988	1/3	2.714	−0.481	0.992
1/2	2.798	−0.730	0.984	1/2	2.920	−0.724	0.974
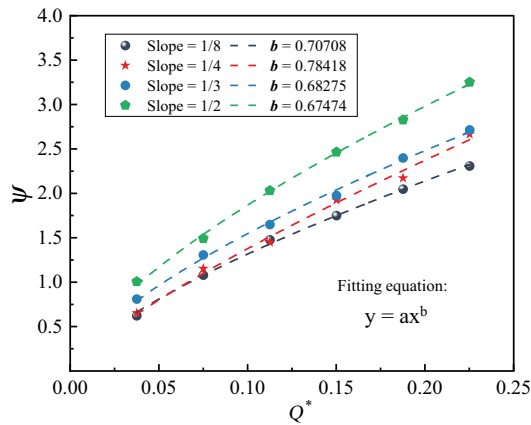
Fig. 18 Variation of coefficient ψ with dimensionless heat release rate Q^*

Fig. 19 Variation of $\psi/Q^{*0.711}$ with slope α

$$\psi = f(\alpha) \cdot Q^{*0.711} \tag{20}$$

Comparing Fig. 18 with Fig. 15, it is found that ψ at different slopes are approximately the same after transformation, and after fitting the exponential function, it is concluded that:

$$\psi/Q^{*0.711} = (5.396 + 0.862e^{3.144\alpha}) \tag{21}$$

$$\gamma = -0.315 - 2.805\alpha^{2.621} \tag{22}$$

The coefficient γ is only related to the slope and is fitted by Fig. 14 to give:

Summarizing Eqs. (21) and (22) into Eq. (16), the maximum excess temperature decay equation downstream of the fire source was obtained as follows:

$$\frac{\Delta T_{max,x}}{T_a} = Q^{*0.711} \cdot \left(5.396 + 0.862e^{3.144\alpha}\right) e^{\left(-0.315 - 2.805\alpha^{2.621}\right)\left(\frac{x}{H_d}\right)} \tag{23}$$

Equation (23) shows that the maximum ceiling excess temperature in the far-field downstream of the fire decays exponentially with the slope of the inclined section. Additionally, the dimensionless maximum temperature rise is proportional to the dimensionless heat release rate 0.711 times, which is similar to the results of previous studies 2/3. Figure 19 shows the data calculated with Eq. (23) compared with the simulated data with an error of no more than 10%, which further verifies the reliability of the formula. However, when the conditions of the inclined section of the utility tunnel are outside the range of slope 1/8–1/2 and fire heat release rate of 0.5–3 MW, Eq. (23) should be used with caution. Figure 20 shows the comparison of the experimental data of four different sizes of pans with the data calculated by Eq. (23), and the error of the calculation increases to 20%
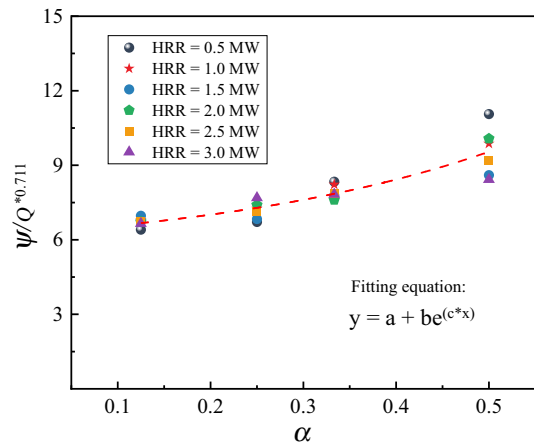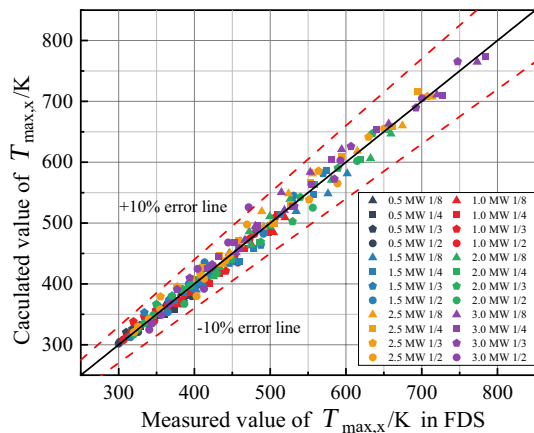

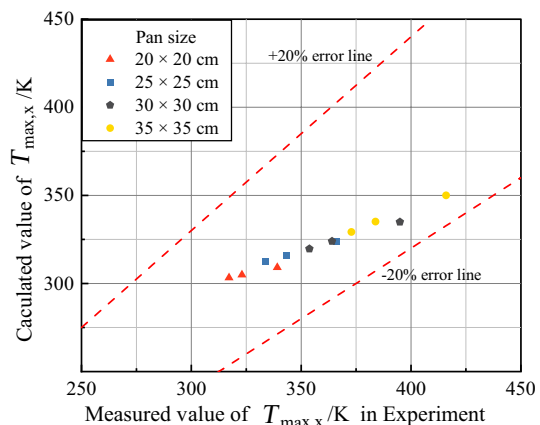**Fig. 20** Comparison of data calculated from Eq. 19 with simulated data

Fig. 21 Comparison of data calculated from Eq. 19 with experimental data

because the power of the fire source is much smaller than that in FDS.

Conclusions

In this study, numerical simulation methods were used to simulate fires in the sunk section of a utility tunnel with slopes of 0, 1/8, 1/4, 1/3 and 1/2. The study is about the smoke movement along the longitudinal centerline and the vertical temperature distribution in the inclined section as well as the downstream longitudinal temperature decay of the utility tunnel fire in conjunction with experiments. The smoke movement and temperature distribution in the sunk area of the utility tunnel are dramatically different compared to the widely studied horizontal utility tunnel. In addition, we conducted experiments in the full-size utility tunnel, and the experimental results were in good agreement with the numerical simulation results, which verified the reliability of the numerical simulation. The main conclusions of this study are as follows:

(1) The stack effect occurs due to the height difference between the two ends of the inclined section of the utility tunnel. Smoke movement has the following main stages: free rise, diffusion under inclined ceiling, diffusion under horizontal ceiling, flow back, and steady diffusion. The smoke downstream of the fire source is approximately parallel to the horizontal line. As the smoke gathers in the upper horizontal section, the high-temperature area is mainly concentrated in the whole upper horizontal section and the ceiling area of the lower horizontal section.

(2) The flame tilts downstream, the temperature downstream from the same horizontal distance from the fire source is lower than the temperature upstream, and the vertical temperature decreases more sharply as the height decreases. As the slope of the inclined section increases, the upstream vertical temperature of the fire source no longer increases when the slope is greater than 1/4, while the downstream vertical temperature gradually decreases.

(3) Based on the simulation data, an empirical formula for the downstream maximum excess ceiling temperature in the sunk area is established. The equation shows that the dimensionless downstream maximum temperature rise decreases as the distance from the fire source increases. It is proportional to the 0.711 power of the dimensionless heat release rate and has a nonlinear and nonmonotonic relationship with the slope of the inclined section.

References

1. Ye K, Zhou X, Zheng Y, et al. Estimating the longitudinal maximum gas temperature attenuation of ceiling jet flows generated by strong fire plumes in an urban utility tunnel. Int J Therm Sci. 2019;142:434–48. https://doi.org/10.1016/j.ijthermalsci.2019.04.023.

2. Cano-Hurtado JJ, Canto-Perello J. Sustainable development of urban underground space for utilities. Tunn Undergr Space Technol. 1999;14(3):335–40. https://doi.org/10.1016/S0886-7798(99)00048-6.

3. Canto-Perello J, Curiel-Esparza J. An analysis of utility tunnel viability in urban areas. Civ Eng Environ Syst. 2006;23(1):11–9. https://doi.org/10.1080/10286600600562129.

4. Wang T, Tan L, Xie S, et al. Development and applications of common utility tunnels in China. Tunn Undergr Space Technol. 2018;76:92–106. https://doi.org/10.1016/j.tust.2018.03.006.

5. Wu J, Bai Y, Fang W, et al. An integrated quantitative risk assessment method for urban underground utility tunnels. Reliab Eng Syst Saf. 2021;213:107792. https://doi.org/10.1016/j.ress.2021.107792.

6. Bai Y, Zhou R, Wu J. Hazard identification and analysis of urban utility tunnels in China. Tunn Undergr Space Technol. 2020;106:103584. https://doi.org/10.1016/j.tust.2020.103584.

7. Piccinini N, Tommasini R, Pons E, Large NG. explosion and fire involving several buried utility networks. Process Saf Environ Protect. 2009;87(2):73–80. https://doi.org/10.1016/j.psep.2008.02.007.

8. Wang P, Zhu G, Pan R, et al. Effects of curved sidewall on maximum temperature and longitudinal temperature distribution induced by linear fire source in utility tunnel. Case Stud Therm Eng. 2020;17:100555. https://doi.org/10.1016/j.csite.2019.100555.

9. Liang K, Hao X, An W, et al. Study on cable fire spread and smoke temperature distribution in T-shaped utility tunnel. Case Stud Therm Eng. 2019;14:100433. https://doi.org/10.1016/j.csite.2019.100433.

10. An W, Tang Y, Liang K, et al. Study on temperature distribution and CO diffusion induced by cable fire in L-shaped utility tunnel. Sust Cities Soc. 2020;62:102407. https://doi.org/10.1016/j.scs.2020.102407.

11. Mi H, Liu Y, Jiao Z, et al. A numerical study on the optimization of ventilation mode during emergency of cable fire in utility tunnel. Tunn Undergr Space Technol. 2020;100:103403. https://doi.org/10.1016/j.tust.2020.103403.

12. Pan R, Zhu G, Liang Z, et al. Experimental study on the fire shape and maximum temperature beneath ceiling centerline in utility tunnel under the effect of curved sidewall. Tunn Undergr Space

Technol. 2020;99:103304. https://doi.org/10.1016/j.tust.2020.103304.

13. Ye K, Tang X, Zheng Y, et al. Estimating the two-dimensional thermal environment generated by strong fire plumes in an urban utility tunnel, Process Saf. Environ Protect. 2021;148:737–50. https://doi.org/10.1016/j.psep.2021.01.030.

14. Gao Z, Li L, Zhong W, et al. Characterization and prediction of ceiling temperature propagation of thermal plume in confined environment of common services tunnel. Tunn Undergr Space Technol. 2021;110:103714. https://doi.org/10.1016/j.tust.2020.103714.

15. Huang P, Ye S, Qin L, et al. Experimental study on the maximum excess ceiling gas temperature generated by horizontal cable tray fires in urban utility tunnels. Int J Therm Sci. 2022;172:107341. https://doi.org/10.1016/j.ijthermalsci.2021.107341.

16. Ji J, Wan H, Li K, et al. A numerical study on upstream maximum temperature in inclined urban road tunnel fires. Int J Heat Mass Tran. 2015;88:516–26. https://doi.org/10.1016/j.ijheatmasstransfer.2015.05.002.

17. Smagorinsky J. General circulation experiments with the primitive equations. Mon Weather Rev. 1963;91(3):99–164.

18. Fan CG, Li XY, Mu Y, et al. Smoke movement characteristics under stack effect in a mine laneway fire. Appl Therm Eng. 2017;110:70–9. https://doi.org/10.1016/j.applthermaleng.2016.08.120.

19. Gao Z, Li L, Sun C, et al. Effect of longitudinal slope on the smoke propagation and ceiling temperature characterization in sloping tunnel fires under natural ventilation. Tunn Undergr Space Technol. 2022;123:104396. https://doi.org/10.1016/j.tust.2022.104396.

20. Han J, Liu F, Wang F, et al. Study on the smoke movement and downstream temperature distribution in a sloping tunnel with one closed portal. Int J Therm Sci. 2020;149:106165. https://doi.org/10.1016/j.ijthermalsci.2019.106165.

21. Mcgrattan KB, Mcdermott RJ, Weinschenk C G, et al. Fire Dynamics Simulator User's Guide, Nist Special Publication; 2013.

22. Karlsson B, Quintiere J G. Enclosure fire dynamics, CRC Press; 2000.

23. Król M, Król A, Koper P, et al. The influence of natural draught on the air flow in a tunnel with longitudinal ventilation. Tunn Undergr Space Technol. 2019;85:140–8. https://doi.org/10.1016/j.tust.2018.12.008.

24. Wang Z, Ding L, Wan H, et al. Numerical investigation on the effect of tunnel width and slope on ceiling gas temperature in inclined tunnels. Int J Therm Sci. 2020;152:106272. https://doi.org/10.1016/j.ijthermalsci.2020.106272.

25. Oka Y, Imazeki O. Temperature and velocity distributions of a ceiling jet along an inclined ceiling – Part 1: approximation with exponential function. Fire Saf J. 2014;65:41–52. https://doi.org/10.1016/j.firesaf.2013.07.009.

26. Oka Y, Oka H, Imazeki O. Ceiling-jet thickness and vertical distribution along flat-ceilinged horizontal tunnel with natural ventilation. Tunn Undergr Space Technol. 2016;53:68–77. https://doi.org/10.1016/j.tust.2015.12.019.

27. Kurioka H, Oka Y, Satoh H, et al. Fire properties in near field of square fire source with longitudinal ventilation in tunnels. Fire Saf J. 2003;38(4):319–40. https://doi.org/10.1016/S0379-7112(02)00089-9.

28. Li YZ, Lei B, Ingason H. The maximum temperature of buoyancy-driven smoke flow beneath the ceiling in tunnel fires. Fire Saf J. 2011;46(4):204–10. https://doi.org/10.1016/j.firesaf.2011.02.002.

29. Hu LH, Chen LF, Wu L, et al. An experimental investigation and correlation on buoyant gas temperature below ceiling in a slopping tunnel fire. Appl Therm Eng. 2013;51(1):246–54. https://doi.org/10.1016/j.applthermaleng.2012.07.043.